Small 11.36 (2015): 4731-4736

DOI: http://dx.doi.org/10.1002/smll.201500874

Magnetic Force Microscopy in Liquids

Pablo Ares, Miriam Jaafar*, Adriana Gil, Julio Gómez-Herrero and Agustina Asenjo*

P. Ares, Prof. J. Gómez-Herrero
Departamento de Física de la Materia Condensada
Universidad Autónoma de Madrid
E-28049 Madrid, Spain
E-mail: pablo.ares@uam.es
Dr. M Jaafar, Dr. A. Asenjo
Instituto de Ciencia de Materiales de Madrid
Consejo Superior de Investigaciones Científicas
E-28049Madrid, Spain
E-mail: m_jaafar@icmm.csic.es
Dr. A. Gil
Nanotec Electrónica S.L.
E-28760 Tres Cantos (Madrid), Spain

Prof. J. Gómez-Herrero
INC and Condensed Matter Physics Center (IFIMAC)
Universidad Autónoma de Madrid
E-28049 Madrid, Spain

Keywords: magnetic force microscopy, liquids, magnetic nanoparticles, nanobiotechnology

In this work, the use of magnetic force microscopy (MFM) to acquire images of magnetic nanostructures in liquid environments is presented. Optimization of the MFM signal acquisition in liquid media is performed and it is applied to characterize the magnetic signal of magnetite nanoparticles. The ability for detecting magnetic nanostructures along with the well-known capabilities of AFM in liquids suggests potential applications in fields such as nanomedicine, nanobiotechnology or nanocatalysis.

1. Introduction

Magnetic nanostructures play an important role innanomedicine, biology or nanocatalysis. The use of magnetic nanoparticles (MNPs) is growing a lot of attention for its potential applications[1] that include contrast enhancement agents for magnetic resonance

imaging, therapeutic drug, gene and radionuclide delivery, methods for the catabolism of tumours via hyperthermia or magnetic separation of labelled cells and other biological entities. Several pathologies such as Alzheimer‘s, Huntington‘s and Parkinson‘s diseases,[2, 3] atherosclerosis[4] and Hepatitis B[5] are characterized for the presence of magnetic deposits in diseased tissue. There are animals, such as the rainbow trout, where a magnetic sense is related to the presence of magnetic nanocrystals for magnetoreception.[6] The encapsulation of magnetic particles in different biological entities is attracting many studies as well: magnetic bacterias[7] to be used as magnetic markers for biosensing,[8] or virus-like cages, which are promising templates for building up nanometric-sized magnetic clusters by taking advantage of their inner cavity as a nanoreactor.[9, 10] Nano-magnetic catalysts are also focusing a lot of attention because they generally avoid loss of catalyst increasing their reusability.[11]

Atomic force microscopy (AFM) is nowadays a powerful technique in biophysiscs,[12, 13] nanomedicine[14] or nanobiotechnology,[15] since it allows imaging and manipulating nanostructures in physiological conditions on a single molecule level.[16, 17] Magnetic force microscopy (MFM) is an AFM-based technique where a nanometric magnetic probe is raster-scanned in close proximity to a surface detecting the local magnetic fields near the surface.[18] MFM has been applied to the study of a variety of magnetic systems,[19] including MNPs,[20-23] but always in vacuum or atmospheric conditions. In particular, Schreiber, *et al*.,[23] commented on the importance of being able to develop MFM imaging in liquid media since biological specimens can dramatically change their properties when studied far away of physiological conditions.

Albeit the high importance of measuring magnetic nanoobjects in biological conditions,the applicability of MFM to biological systems has been limited up to now because of the difficulty in developing MFM for detecting magnetic interactions in liquids,[23] as a consequence of the high damping forces on the cantilever, which are several times greater than in air. This is the origin of the low quality factor (Q) of the cantilever resonance

characteristic of liquid measurements. This low Q results in a significant loss of sensitivity in the MFM signal. Giles *et al*. recorded bits on a computer hard disk in air and in liquid,[24] but in their study topography was acquired with the tip in contact mode. This is unacceptable for the majority of biological applications, where the biological specimens under consideration are weakly immobilized to a flat surface,[8] because the tip will destroy the sample. In addition, they optimized the magnetic contrast by changing the pH of the liquid in order to change the adhesion and the attractive forces to measure as close as possible to the surface. This can be again unaceptable for many biological applications, where the biological specimens need to be under specific buffer conditions. More recently, Dietz *et al*. reported the detection of superparamagnetic particles in liquid using bimodal AFM.[25] In this case the contrast obtained is not purely magnetic but a cross-talk of nanomechanical and magnetic interactions.

In this work, we have studied the tip-sample magnetic interaction in different media (high vacuum, air and liquids) using magnetic hard disk drives as a benchmark and we have highly optimized the acquisition conditions in liquid environment. In order to explore the final sensitivity of MFM in liquids we also present imaging of Fe_3O_4 MNPs coated with dimercaptosuccinnic acid (DMSA) in both air and liquid environments. DMSA-coated MNPs are promising nanostructures for different nanomedicine applications due to their biocompatibility and low toxicity.[26] We compare the magnetic contrast obtained vs. the amount of magnetic material measured in air and liquid. Despite a reduction in the signal-to-noise ratio, the magnetic contrast can be seen as well showing a good lateral resolution. The potential of the technique for detecting and imaging nanoscale magnetic domains in biological samples using MFM is discussed.

2. Results and discussion

2.1. MFM contrast optimization in liquids: hard disk drives

We start by imaging the magnetic domains of a high density disk drive using commercial MFM probes in both air and liquid environments.

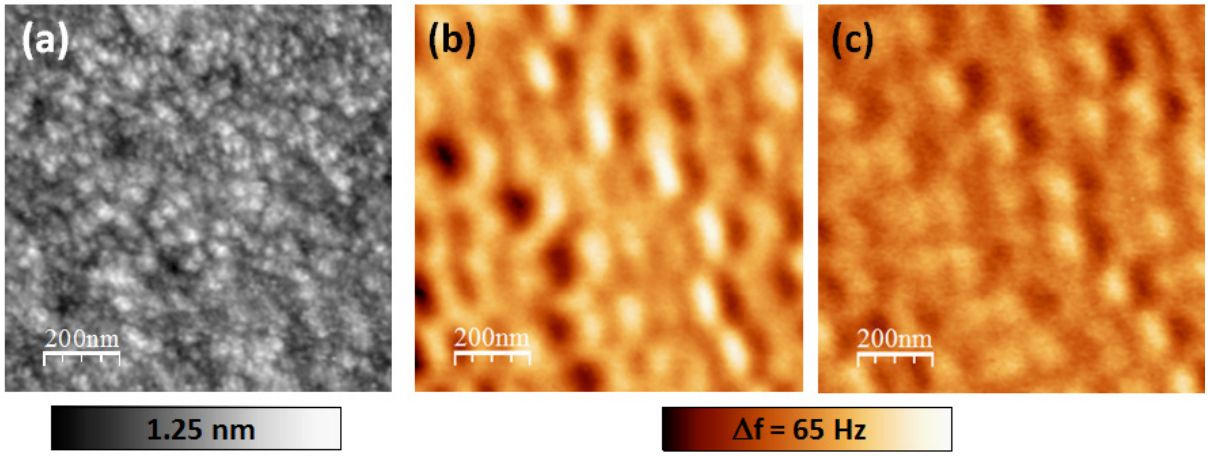

Figure 1. (a) High density hard disk surface topography. Cantilever amplitude = 5 nm. (b) MFM image of the hard disk taken in ambient air conditions. Z lift = 15 nm. (c) MFM image taken in liquid. Z lift = 6 nm. Please note the scanned area is not the same as in (b).

Figure 1 shows the topography and magnetic contrast obtained from the frequency shift in both media in a double-pass configuration (see *MFM studies* in the experimental section for details). As expected, the image acquired in air (Figure 1b) presents a more marked contrast than the one in liquid (Figure 1c), but still the lateral resolution and sensitivity of the *in-liquid* image is good enough as to easily resolve the ~ 60 nm domains. Notice that the same color scale has been used in both magnetic images in order to compare them readily. No topography cross-talk is observed along the MFM images (see Figure S1 in the Supporting Information for a comparison of topography and frequency shifts in 1st and 2nd passes in both air and liquid media). This lower magnetic signal is a direct consequence of the low Q factor of the cantilever resonance characteristic of liquid measurements (see **Figure 2a**). The origin of the magnetic contrast can be better understood by monitoring the variation of the interaction with the tip-sample distance. To this end, the tip is moved along a given line parallel to the

domains transition direction (in a similar way as a magnetic reader head does), so MFM contrast given by the cantilever resonance frequency shift can be readily studied at different lift heights in a fast and drift-free way. The result of this acquisition scheme is called 3D mode mapping[27] (Figure 2b). The frequency shift induced by the magnetic interaction at different Z lifts is recorded, showing attractive and repulsive contrast (bright and dark areas, Figure 2c). If this same process is carried out in air and vacuum we can plot the magnetic interaction in the different media as a function of the distance for both the attractive and repulsive areas (Figure 2d). Figure 2e shows a plot of different frequency shift profiles as a function of Z lift. In this plot it can be easily seen how the topographic information fades away as the Z lift increases, thus allows choosing the optimal Z lift distance for MFM imaging with no topography cross-talk.

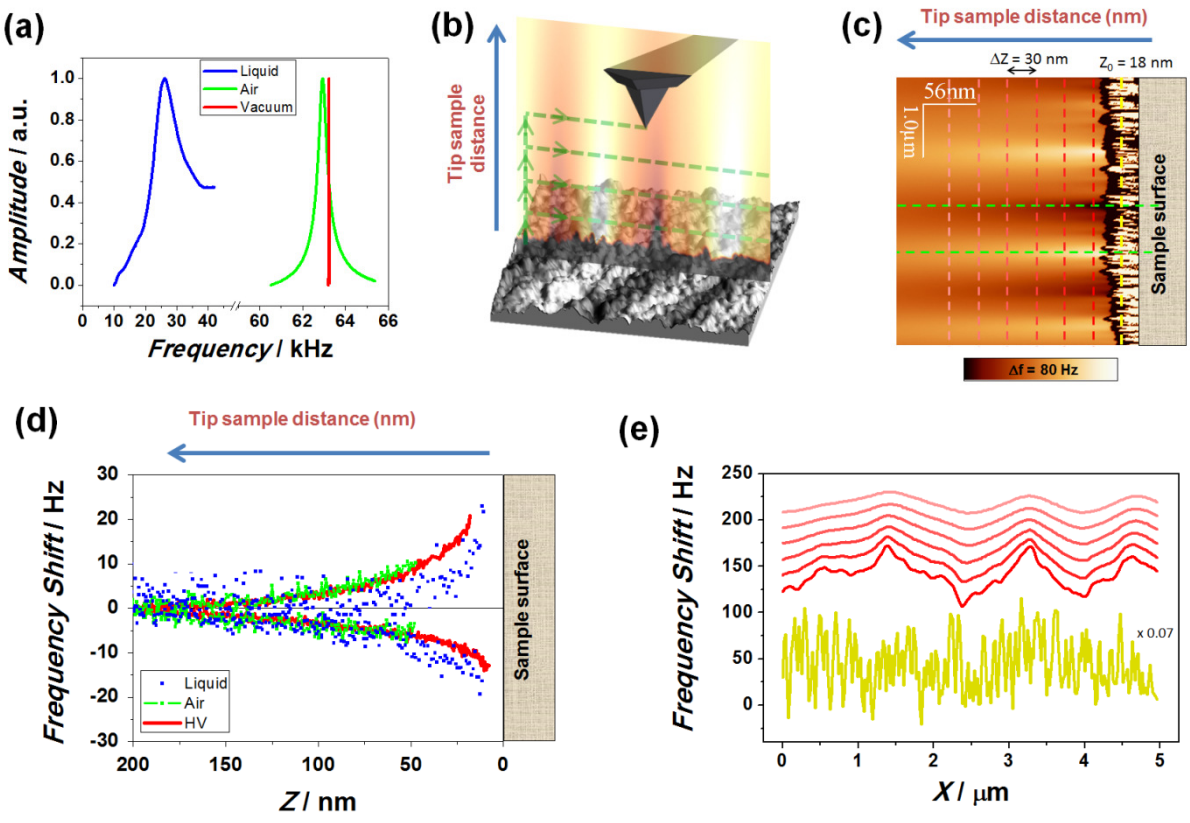

Figure 2. (a) Cantilever Nanosensors™ PPP-MFMR resonance curves in different media: liquid, ambient air and High Vacuum (HV). (b) Scheme of the 3D mode measurement of the magnetic interaction as a function of the tip-sample distance. (c) 3D mode map obtained in ambient air conditions showing the magnetic contrast along a given scanning line as a function of the Z lift in a low density hard disk sample. (d) Magnetic signal from attractive

and repulsive regions of the hard disk in the different media taken from 3D modes similar to that shown in (c). The regions taken in each media correspond to the positions showing higher attractive and repulsive contrasts as marked by the horizontal dashed green lines in (c). (e) Frequency shift vs. X distance along the scanning line for different Z lifts according to the vertical lines in (c). The yellow line has been divided by a factor of 15 for visibility. All lines have been arbitrarily shifted for visibility.

As expected from the Q factor values, the high vacuum signals are the cleanest ones, whereas the liquid signals are the noisiest. But interestingly, it can be observed that in both vacuum and liquid, where the attractive forces are much lower than in air,[28] the magnetic signal can be detected with the tip very close to the sample (tip sample distances < 10 nm), in contrast to air conditions, where the minimum distance to detect magnetic interaction with no topography cross-talk is much higher due to the presence of capillary forces (see Figure S2 for a representative example). To optimize the magnetic contrast in liquids, we have done this kind of analysis for different oscillation amplitudes and different dynamic modes: Amplitude Modulation, AM-AFM and Drive Amplitude Modulation, DAM-AFM[29] in both air and liquid. DAM-AFM follows a similar feedback scheme as Frequency Modulation, FM-AFM, but the main topography feedback is done on the drive amplitude signal (dissipation channel). In terms of the acquisition of magnetic interactions, it is the same as FM-AFM, but since there are no frequency shift contributions to the topography, it has the advantage of avoiding any magnetic cross-talk in the first pass topography acquisition (as already mentioned in the supporting information of [29]). We have maximized the MFM signal studying the influence of the relevant operating parameters in both AM-AFM and DAM-AFM modes. For a given measuring condition (for example the cantilever oscillation amplitude) we varied the other relevant operating conditions (such as Set point, Z lift distance or Phase Lock Loop parameters) to maximize the MFM signal. We have found that by working in DAM-AFM, the tip can detect the magnetic interaction closer to the sample, which translates into a higher magnetic contrast (see Figure S3 in the Supporting Information). Thus, despite the loss in sensitivity in liquid compared to air, similar contrasts can be achieved (as shown in Figure 1b

and Figure 1c) using the most appropriated oscillation amplitudes and tip-sample distances for every mode and medium.

2.2. DMSA-coated Fe_3O_4 MNPs

DMSA-coated Fe_3O_4 ferrimagnetic NPs were deposited onto freshly cleaved mica (see the experimental section for details).

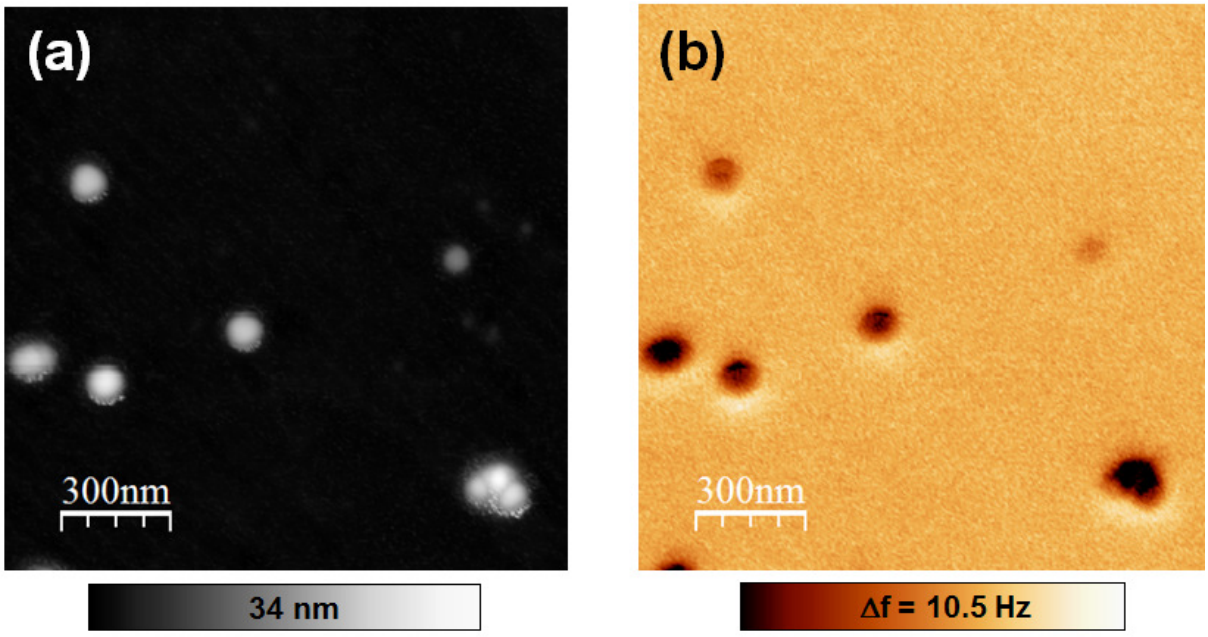

Figure 3. (a) Topography and (b) MFM image of (DMSA)-coated Fe_3O_4 nanoparticles acquired in ambient air conditions. Z lift = 15nm.

Figure 3 shows the topography and magnetic contrast in air conditions of a typical distribution of MNPs on the substrate, presenting single particles and clusters comprising several particles. Albeit the cubic shape of the nanoparticles, the AFM images give us spherical features due to the tip-sample dilation. MNPs were magnetized in the in plane direction by means of a permanent magnet prior to the measurements Due the magnetocrystalline anisotropy, the magnetization lies along one of the easy axis of the particle.[30] This is reflected as a bright-dark contrast (Figure 3 and **Figure 4**) coming from the magnetic dipole response.[22, 23] Note that the ratio between magnetic signals in the hard disks

and MNPs is about an order of magnitude. Figure 4 shows topography and magnetic images of single MNPs and clusters measured in both air and liquid. The magnetic contrast in air can be readily seen in all the cases, matching the state of the art images for this kind of systems.[21-23, 31] Moreover, despite of the low magnetic signal-to-noise ratio characteristic of liquids, we can still measure the magnetic contrast in the case of particles as low as~ 30 nm, which is in the limit of the technique, with negligible topography cross-talk (see Figure S4 for details).

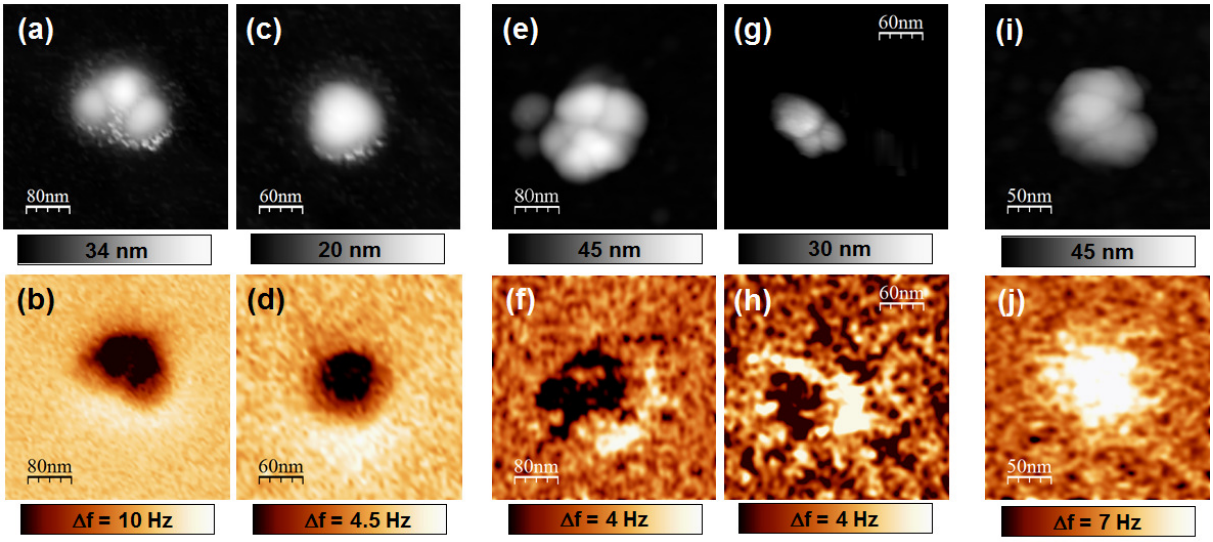

Figure 4. (a,, c, e, g, i) Topography and (b, d, f, h, j) 2nd pass frequency shift images of (DMSA)-coated Fe_3O_4 nanoparticles. (a-d) Images acquired in ambient air conditions. Z lift = 15nm. (e-j) Images acquired in liquid. Z lift = 6 nm. (a-h) were acquired using a MFM tip, whereas (i, j) were acquired using a probe with similar characteristics but without magnetic coating.

As the spatial dependence of both magnetic and electrostatic interactions in AFM is similar, it is fundamental to demonstrate the magnetic origin of the signal measured in the nanoparticles.[32, 33] To this end, we carried out measurements in liquids in exactly the same conditions using cantilevers with similar characteristics as the MFM ones, but with a metallic non-magnetic coating. In these cases, the dark-bright contrast does not appear (Figure 4j).

We can compare the magnetic signal for each of the particles and clusters observed by measuring the difference between the dark and the bright contrast. **Figure 5** shows the

comparison between the measured magnetic signal of the MNPs in both air and liquid as a function of the volume of the MNP, i.e. as a function of the magnetic material present. Remarkably, despite the increase of the noise in the liquid measurements due to the low Q factor of the cantilever resonance, we can still obtain similar magnetic contrasts in liquid than in air.

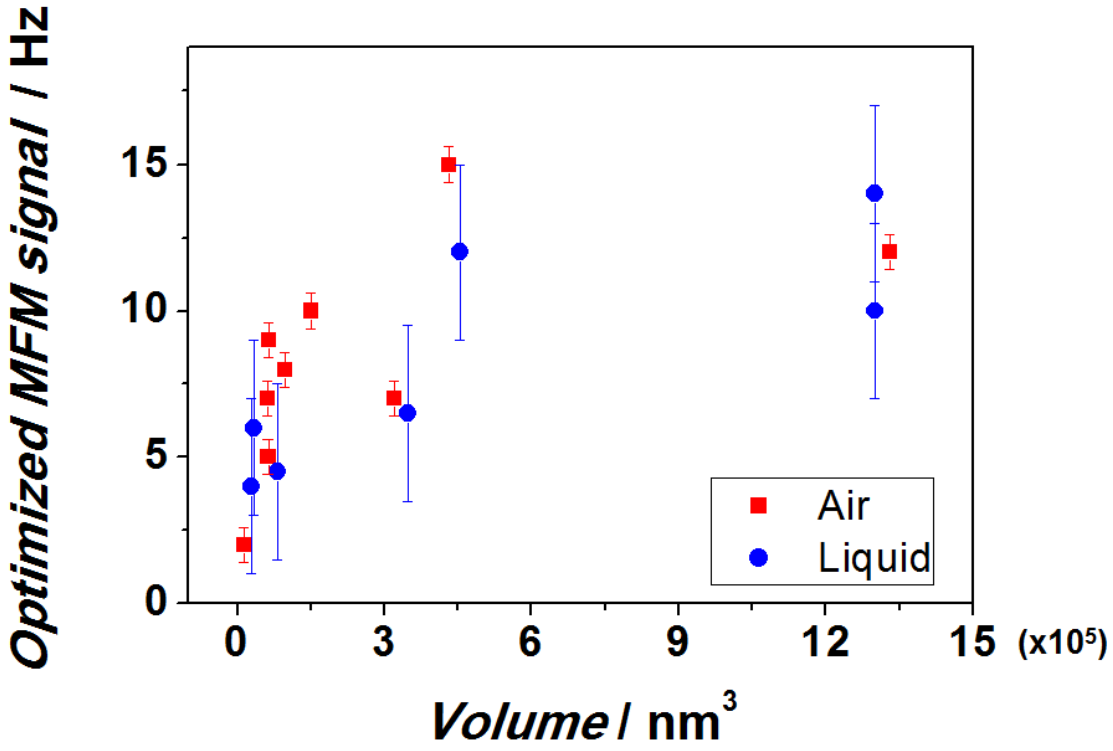

Figure 5. Magnetic contrast as a function of the amount of magnetic material in the (DMSA)-coated Fe_3O_4 nanoparticles for both air and liquid measurements.

In this work we have demonstrated the feasibility of using the MFM technique in liquid environments. MFM studies in liquids have been carried out using DAM-AFM mode and commercial MFM probes, being able to detect magnetic signals even from a single 30-nm Fe_3O_4 nanoparticle. This was possible by fine tuning of the experimental setup including the use of a specially designed cantilever holder with clean resonance peaks in liquid (see experimental section for details). Imaging the surface using DAM-AFM mode was important as well since it allows optimization of the magnetic contrast by being able to detect it closer to

the sample. Regarding probes, a simple study of fundamental MFM noise shows that further improvement on the performance could be gained through the use of specially designed cantilevers for liquid media (see Supporting Information, *MFM probes customization for liquid environments* section).

4. Conclusions

In summary, we have demonstrated the applicability of the MFM as a means of detecting magnetic nanostructures in liquid environments. We have optimized the measuring conditions by using hard disk drives and we have studied DMSA-coated Fe_3O_4 nanoparticles. Despite the limiting factor of the low magnetic interactions, we have presented clear evidence showing that even individual 30-nm MNPs can be detected using commercial probes. These results suggest new strategies for the characterization of magnetic nanostructures in liquids using MFM.

5. Experimental Section

Materials: Low and high density magnetic hard disk drive samples were obtained by cutting pieces of ~1 cm^2 from hard disk drives with magnetic motives of ~800 nm and ~60 nm respectively.

Fe_3O_4 MNPs coated with dimercaptosuccinnic acid (DMSA) were obtained by precipitation of a $FeSO_4$ solution in a basic solution in the presence of potassium nitrate (acting as mild oxidant) under stirring and nitrogen flow. The precipitate is then placed in an oil bath at 90 ºC with mechanical stirring for 15 min and left tightly closed for 24 h without agitation.[34] Finally the particles were coated with DMSA at pH 3 and the excess removed after two days dialysis. Magnetite particles obtained by this route present an inverse spinel structure and ferrimagnetic behavior at room temperature with very high saturation magnetization values.[34]

Mica substrates (muscovite V-1 quality) were used to deposit the MNPs.

MFM studies: For the hard disk drive samples studies in liquid, distilled water was deposited on the disk drive surface. For the MNPs, a solution of 2.4 mg Fe/ml of MNPs was diluted in the range 1:5 in a 5mM nickel chloride solution to ensure proper MNPs immobilization just before use and immediately aliquoted onto freshly cleaved mica. After 20 minutes, the mica substrates were dried in a N_2 gas jet and imaged in air conditions. For MNPs studies in liquids, distilled water was added to the mica substrates with MNPs previously imaged.

The samples were imaged using a Cervantes FullMode AFM from Nanotec Electrónica, equipped with a Dolphin cantilever holder, a holder specially designed to work in liquids using acoustic excitation avoiding the spurious resonances known as 'forest of peaks'.[35] Figure S5 in the Supporting Information shows a typical frequency resonance curve of a MFM probe in liquid, together with its thermal spectrum and the ideal cantilever response for acoustic excitation, showing an excellent agreement. For the high vacuum measurements, the microscope was placed in a home-made vacuum chamber with a base pressure of 10^{-6} mbar. Data acquisition and processing were carried out through the WSxM software (www.wsxmsolutions.com).[36] Commercial MFM probes PPP-MFMR from Nanosensors™ (www.nanosensors.com) were employed. PPP-MFMR probes have a cantilever length of 225 µm with a resonant frequency of 75 kHz and a typical force constant of 2.8 $N \cdot m^{-1}$. The tip has a hardmagnetic coating and a radius of curvature < 30 nm. The coating is characterized by a coercivity of ~ 300 Oe. For enhanced signal strength probes were magnetized by means of a strong permanent magnet prior to the measurements.

MFM imaging was performed in different dynamic modes: Amplitude Modulation AM-AFM mode and Drive Amplitude Modulation mode DAM-AFM. A Phase Lock Loop (PLL) integrated in the Cervantes AFM was used to keep the cantilever in resonance, measuring the frequency shift. The interaction between the magnetic moments of the tip and the sample, F_z,

induces a change in the resonance frequency of the cantilever with the distance z. This frequency shift (Δω) can be correlated with the force gradient as is shown in **Equation 1**:

$$\Delta\omega = -\frac{\omega_0}{2k}\frac{\partial F_z}{\partial z} \quad (1)$$

Where ω_0 is the resonance frequency and k is the force constant of the cantilever. MFM experiments were recorded by interleaving the topographic scan with the so-called 'Lift Mode' scan, in which the AFM tip was made to scan the sample as a free-standing cantilever with no topography feedback active. The frequency shift measured in this second pass, far away from the surface, is a measure of the tip-sample magnetic interaction. For MFM data analysis, the frequency shift contrast was measured for individual magnetic domains using the analysis section of WSxM.

Acknowledgements
The authors would like to thank M.P. Morales from the ICMM (Madrid, Spain) for providing the MNPs and for careful reading of the manuscript. This work was supported by Consolider CSD2010-0024, MAT2013-46753-C2-2-P and MAT2013-48054-C2-1 projects.

1. Q. A. Pankhurst, J. Connolly, S. K. Jones, J. Dobson, *Journal of Physics D-Applied Physics* **2003,** *36*, R167.
2. J. Dobson, *FEBS Lett.* **2001,** *496*, 1.
3. M. Savoiardo, F. Girotti, L. Strada, E. Ciceri, *Journal of neural transmission. Supplementum* **1994,** *42*, 93.
4. X.-M. Yuan, W. Li, *Current Medicinal Chemistry* **2008,** *15*, 2157.
5. A. L. Martinelli, A. B. Araujo, R. F. Franco, M. H. Tavella, L. N. Z. Ramalho, S. Zucoloto, S. S. Rodrigues, M. A. Zago, *Journal of Gastroenterology and Hepatology* **2004,** *19*, 1036.
6. C. E. Diebel, R. Proksch, C. R. Green, P. Neilson, M. M. Walker, *Nature* **2000,** *406*, 299.
7. M. Martin, F. Carmona, R. Cuesta, D. Rondon, N. Galvez, J. M. Dominguez-Vera, *Adv. Funct. Mater.* **2014,** *24*, 3489.
8. Y. Amemiya, T. Tanaka, B. Yoza, T. Matsunaga, *J. Biotechnol.* **2005,** *120*, 308.
9. A. A. A. Aljabali, F. Sainsbury, G. P. Lomonossoff, D. J. Evans, *Small* **2010,** *6*, 818.
10. M. Jaafar, A. A. A. Aljabali, I. Berlanga, R. Mas-Balleste, P. Saxena, S. Warren, G. P. Lomonossoff, D. J. Evans, P. J. de Pablo, *Acs Applied Materials & Interfaces* **2014,** *6*, 20936.
11. S. Hu, Y. Guan, Y. Wang, H. Han, *Applied Energy* **2011,** *88*, 2685.
12. A. Alessandrini, P. Facci, *Measurement Science & Technology* **2005,** *16*, R65.

13. N. C. Santos, M. Castanho, *Biophys. Chem.* **2004,** *107*, 133.
14. D. Nikova, T. Lange, H. Oberleithner, H. Schillers, A. Ebner, P. Hinterdorfer, Atomic force microscopy in nanomedicine, in *Applied Scanning Probe Methods III: Characterization*, (Eds: B. Bhushan, H. Fuchs), **2006**, pp. 1-26.
15. D. J. Mueller, Y. F. Dufrene, *Nature Nanotech.* **2008,** *3*, 261.
16. D. Fotiadis, Y. Liang, S. Filipek, D. A. Saperstein, A. Engel, K. Palczewski, *Nature* **2003,** *421*, 127.
17. M. Rief, M. Gautel, F. Oesterhelt, J. M. Fernandez, H. E. Gaub, *Science* **1997,** *276*, 1109.
18. Y. Martin, H. K. Wickramasinghe, *Appl. Phys. Lett.* **1987,** *50*, 1455.
19. L. Yue, S.-H. Liou, Magnetic Force Microscopy Studies of Magnetic Features and Nanostructures, in *Scanning Probe Microscopy in Nanoscience and Nanotechnology 2*, (Eds: B. Bhushan), Springer Berlin Heidelberg, **2011**, pp. 287-319.
20. S. Block, G. Gloeckl, W. Weitschies, C. A. Helm, *Nano Lett.* **2011,** *11*, 3587.
21. C. S. Neves, P. Quaresma, P. V. Baptista, P. A. Carvalho, J. P. Araujo, E. Pereira, P. Eaton, *Nanotechnology* **2010,** *21*, 305706.
22. T. M. Nocera, J. Chen, C. B. Murray, G. Agarwal, *Nanotechnology* **2012,** *23*, 495704.
23. S. Schreiber, M. Savla, D. V. Pelekhov, D. F. Iscru, C. Selcu, P. C. Hammel, G. Agarwal, *Small* **2008,** *4*, 270.
24. R. Giles, J. P. Cleveland, S. Manne, P. K. Hansma, B. Drake, P. Maivald, C. Boles, J. Gurley, V. Elings, *Appl. Phys. Lett.* **1993,** *63*, 617.
25. C. Dietz, E. T. Herruzo, J. R. Lozano, R. Garcia, *Nanotechnology* **2011,** *22*, 043044.
26. M. Calero, L. Gutierrez, G. Salas, Y. Luengo, A. Lazaro, P. Acedo, M. Puerto Morales, R. Miranda, A. Villanueva, *Nanomedicine-Nanotechnology Biology and Medicine* **2014,** *10*, 733.
27. C. Gomez-Navarro, A. Gil, M. Alvarez, P. J. De Pablo, F. Moreno-Herrero, I. Horcas, R. Fernandez-Sanchez, J. Colchero, J. Gomez-Herrero, A. M. Baro, *Nanotechnology* **2002,** *13*, 314.
28. N. Garcia, V. T. Binh, *Physical Review B* **1992,** *46*, 7946.
29. M. Jaafar, D. Martinez-Martin, M. Cuenca, J. Melcher, A. Raman, J. Gomez-Herrero, *Beilstein Journal of Nanotechnology* **2012,** *3*, 336.
30. C. Moya, O. Iglesias-Freire, N. Pérez, X. Batlle, A. Labarta, A. Asenjo, *Nanoscale* **2015,** *7*, 8110.
31. T. Haeberle, F. Haering, H. Pfeifer, L. Han, B. Kuerbanjiang, U. Wiedwald, U. Herr, B. Koslowski, *New Journal of Physics* **2012,** *14*, 043044.
32. M. Jaafar, O. Iglesias-Freire, L. Serrano-Ramon, M. Ricardo Ibarra, J. Maria de Teresa, A. Asenjo, *Beilstein Journal of Nanotechnology* **2011,** *2*, 552.
33. D. Martinez-Martin, M. Jaafar, R. Perez, J. Gomez-Herrero, A. Asenjo, *Phys. Rev. Lett.* **2010,** *105*, 257203.
34. M. Marciello, V. Connord, S. Veintemillas-Verdaguer, M. Andres Verges, J. Carrey, M. Respaud, C. J. Serna, M. Puerto Morales, *Journal of Materials Chemistry B* **2013,** *1*, 5995.
35. C. Carrasco, P. Ares, P. J. de Pablo, J. Gomez-Herrero, *Rev. Sci. Instrum.* **2008,** *79*, 126106.
36. I. Horcas, R. Fernandez, J. M. Gomez-Rodriguez, J. Colchero, J. Gomez-Herrero, A. M. Baro, *Rev. Sci. Instrum.* **2007,** *78*, 013705.